JVL Formulation (draft)

Mark Drela, MIT Aero & Astro

July 2007

This document gives the theoretical formulation of JVL, which is a program for analysis of arbitrary 3-D aircraft configurations with powered lift, using an extended Vortex-Lattice method. The extensions include

- Effects of rotation rates.
- Effects of control deflections.
- Effects of powered lift via jet blowing.
- Addition of viscous drag forces.
- General force and moment trim capability.

Some of these features have been developed previously, as summarized by Katz and Plotkin [1], and have been implemented in AVL (`http://web.mit.edu/drela/Public/web/avl/`), which is the precursor to JVL. The incorporation of jet blowing and approximate viscous separation influence are new developments in JVL.

Nomenclature

xyz	cartesian coordinates
$\mathbf{r}$	field point ($= x\hat{\mathbf{x}} + y\hat{\mathbf{y}} + z\hat{\mathbf{z}}$)
$\mathbf{r}_i$	location of i'th control point
$\mathbf{r}'_i$	location of i'th vortex leg midpoint
$\mathbf{F}$	aerodynamic force
$\mathbf{M}$	aerodynamic moment
Γ_i	horseshoe vortex circulation
$\mathcal{D}_l$	control surface deflection variable
$\mathcal{P}_l$	jet excess momentum variable
σ	slender body source/length
$\boldsymbol{\nu}$	slender body doublet/length
ρ	freesteam density
μ	freestream viscosity
a	freestream speed of sound
c	local chord
c_ℓ	local lift coefficient
c_d	local profile drag coefficient
c_J	local jet momentum flow coefficient
c_Q	local jet mass flow coefficient
$\mathbf{V}$	freestream velocity ($= V_1\hat{\mathbf{x}} + V_2\hat{\mathbf{y}} + V_3\hat{\mathbf{z}}$)
$\boldsymbol{\Omega}$	aircraft rotation rate ($= \Omega_1\hat{\mathbf{x}} + \Omega_2\hat{\mathbf{y}} + \Omega_3\hat{\mathbf{z}}$)
$\mathbf{w}$	induced velocity of sources and doublets
$\mathbf{v}$	induced velocity of bound and trailing vorticity
$\hat{\mathbf{w}}$	unit-freestream influence coefficient on $\mathbf{w}$
$\hat{\mathbf{v}}$	unit-circulation influence coefficient on $\mathbf{v}$
$\mathbf{W}$	total velocity relative to surface
V	freestream speed ($= \lvert\mathbf{V}\rvert$)
$\hat{\mathbf{V}}$,$\hat{\mathbf{Y}}$,$\hat{\mathbf{L}}$	wind-axes unit vectors
$\hat{\mathbf{n}}$	unit normal vector on surface or jet sheet
h_{jet}	jet sheet height
$\dot{m}'$	jet mass flow/span ($= \int \rho_{\text{jet}} u_{\text{jet}}\, \mathrm{d}n$)
J'	jet momentum/span ($= \int \rho_{\text{jet}} u_{\text{jet}}^2\, \mathrm{d}n$)
$\Delta J'$	jet excess momentum/span ($= J' - \rho V^2 h_{\text{jet}}$)
$\bar{J}$	normalized jet momentum excess ($= \Delta J'/\rho V^2$)
$\dot{m}$	total jet mass flow ($= \int \dot{m}'\, \mathrm{d}\ell$)
J	total jet momentum ($= \int J'\, \mathrm{d}\ell$)
ℓ	distance along span, body, or vortex

1 Configuration Geometry

The geometry to be analyzed consists of thin surfaces of arbitrary planform, together with slender bodies. The surfaces trailing vortex sheets, possibly superimposed with propulsive jet sheets with nonzero excess momentum.

1.1 Surfaces

A surface is defined by two or more *sections* distributed across the span, as shown in Figure 1.1. Each section has the following properties:

- leading edge x, y, z location
- chord
- camberline shape, with incidence angle bias
- control surface hinge location and control gains
- jet excess-momentum control gains
- jet thickness

The surface geometry is linearly interpolated between the sections.

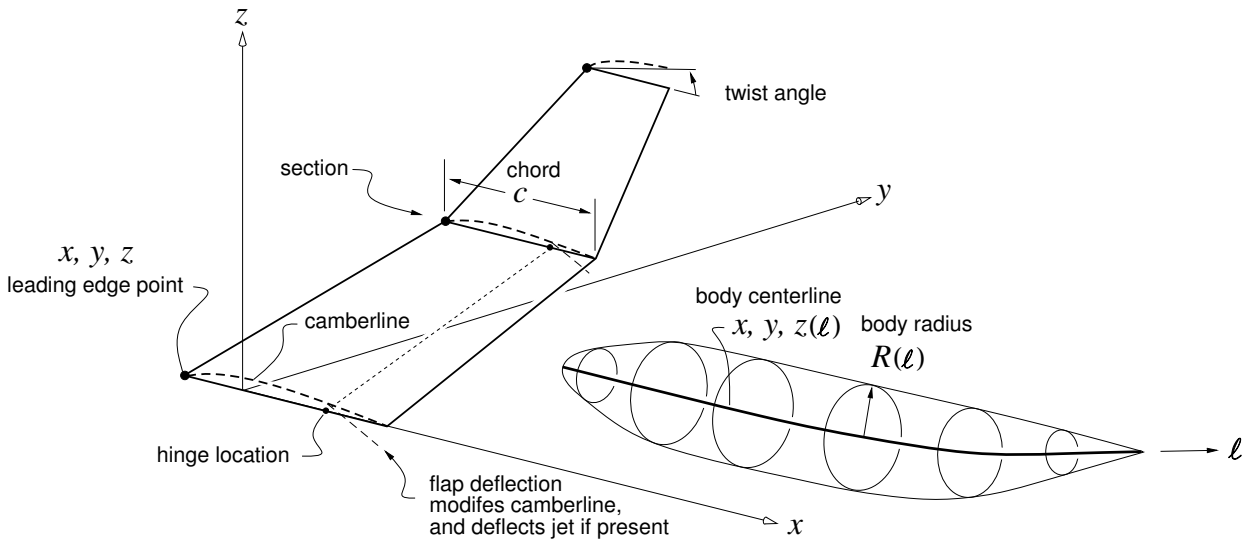

Figure 1: A surface defined by three sections, and a body defined by centerline and radius distributions.

1.2 Bodies

A body is defined by its centerline shape, specified parametrically as $x(\ell), y(\ell), z(\ell)$, and also by the radius distribution $R(\ell)$.

2 Vortex Lattice

2.1 Surface Vortex Discretization

Following established Vortex-Lattice practice [1], Figure 2.1 shows a surface divided into panels, each of which receives a horseshoe vortex of strength Γ_i, and a control point at location $\mathbf{r}_i$. In addition, the present extension models the effects of a propulsive and/or lift-augmenting jet distributed over the span. Such a jet can carry an aerodynamic load (or pressure jump to be more precise), and hence modeling its effect on the potential flow requires also placing horseshoe vortices on the jet sheet, as shown in Figure 2.1.

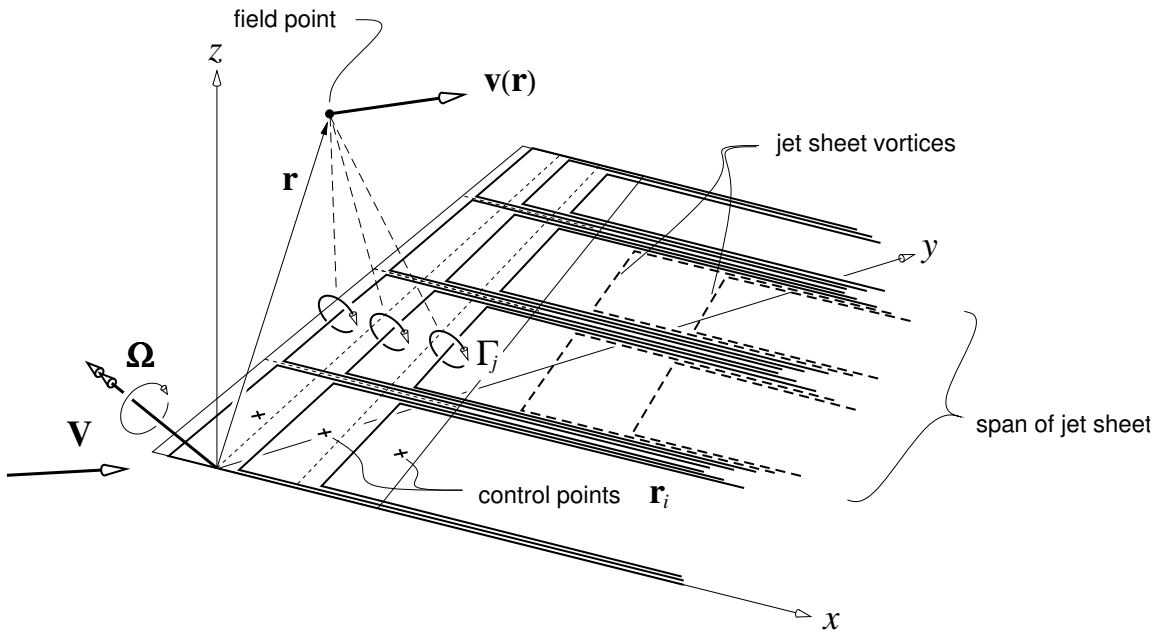

Figure 2: Lattice of horseshoe vortices on a surface, and on jet sheet (if any).

As shown by Lan [2], the best accuracy is obtained if the vortex and control point are shifted by 1/4 of the panel chord (in cosine spacing) towards the trailing edge, as shown in Figure 2.1. A cosine spanwise distribution for the trailing vortex legs and control points also gives best accuracy, and is typically used if possible. Using the discrete ξ and η values pictured in Figure 2.1, the

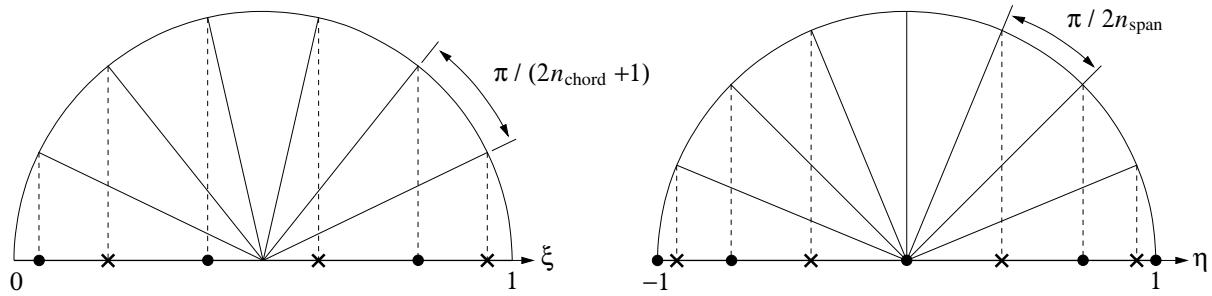

Figure 3: Chordwise and spanwise locations of vortices and control points using cosine spacing.

chordwise and spanwise locations are determined as follows.

$$x = x_{LE} + c\xi \qquad \text{(surface)} \tag{1}$$

$$x = x_{TE} + c\,\frac{\xi}{1-\xi/(1+c/2b_{\text{ref}})} \qquad \text{(jet sheet)} \tag{2}$$

$$y = y_{\text{center}} + \frac{b}{2}\,\eta \tag{3}$$

The jet sheet streamwise spacing distribution above puts the downstream end of the sheet a distance of $2b_{\text{ref}} + c$ behind the trailing edge, where b_{ref} is the reference span, typically the largest span

in the configuration. This is modest distance is actually sufficiently large to render the jet sheet effectively infinite in length, since the jet sheet strength decreases rapidly downstream.

2.2 Body Source and Doublet Discretization

A body is modeled with source plus doublet distributions along its centerline. The distributions are assumed to be piecewise-constant, in a specified number of segments. The segment distribution is arbitrary, although a simple uniform distribution is satisfactory in most cases.

3 Flowfield velocities

3.1 Velocity decomposition

As shown in Figure 2.1, the configuration sees a uniform freestream velocity $\mathbf{V}$, as it rotates at some rotation rate Ω. The total velocity $\mathbf{W}$ relative to a field point $\mathbf{r}$ on a surface is therefore

$$\mathbf{W} \;=\; \mathbf{v} + \mathbf{w} + \mathbf{V} - \mathbf{\Omega} \times \mathbf{r} \tag{4}$$

where the $\mathbf{v}$ velocity is due all the bound and trailing vorticity, including the vorticity on the jet sheet, and $\mathbf{w}$ is the induced velocity of all the volume sources and doublets.

3.2 Velocity field of vortex segment

A horseshoe vortex is defined by its two vertices $\mathbf{r}_a$ and $\mathbf{r}_b$, with circulation defined positive by righthand rule about the bound-vortex vector $\mathbf{r}_b - \mathbf{r}_a$.

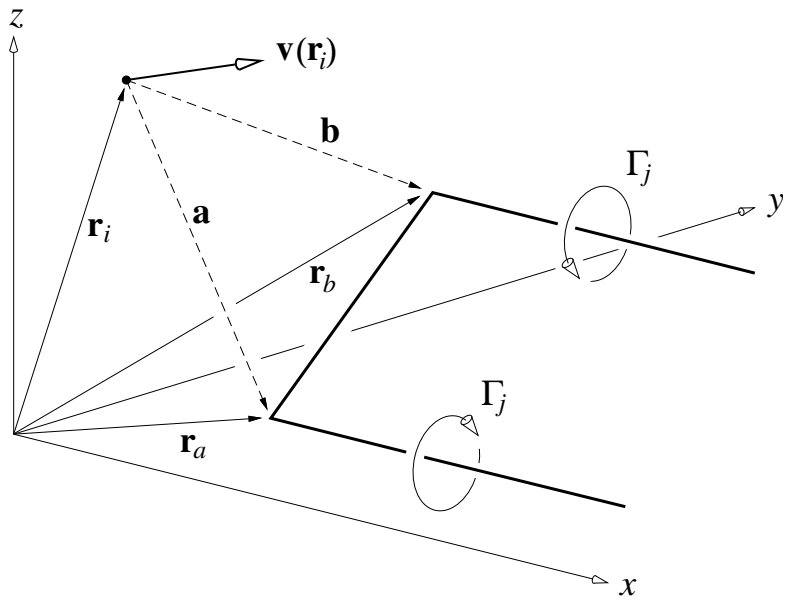

Figure 4: Horseshoe vortex, defined by its vertices $\mathbf{r}_a$ and $\mathbf{r}_b$

The induced velocity at field point $\mathbf{r}_i$ of the j'th horseshoe vortex is then obtained by evaluating

the Biot-Savart integral over the bound vortex segment and the two trailing vortex segments.

$$\mathbf{v}(\mathbf{r}_i) \;=\; \frac{\Gamma}{4\pi}\int \frac{(\mathbf{r}(\ell)-\mathbf{r}_i)\times \mathrm{d}\boldsymbol{\ell}}{|\mathbf{r}(\ell)-\mathbf{r}_i|^3} \;=\; \sum_j \hat{\mathbf{v}}_{ij}\,\Gamma_j \tag{5}$$

$$\text{where}\quad \hat{\mathbf{v}}_{ij} \;=\; \frac{1}{4\pi}\left\{ \frac{\mathbf{a}\times\mathbf{b}}{|\mathbf{a}||\mathbf{b}|+\mathbf{a}\cdot\mathbf{b}}\left(\frac{1}{|\mathbf{a}|}+\frac{1}{|\mathbf{b}|}\right) - \frac{\mathbf{a}\times\hat{\mathbf{x}}}{|\mathbf{a}|+\mathbf{a}\cdot\hat{\mathbf{x}}}\,\frac{1}{|\mathbf{a}|} + \frac{\mathbf{b}\times\hat{\mathbf{x}}}{|\mathbf{b}|+\mathbf{b}\cdot\hat{\mathbf{x}}}\,\frac{1}{|\mathbf{b}|}\right\} \tag{6}$$

$$\mathbf{a} \;=\; \mathbf{r}_a \,-\, \mathbf{r}_i \tag{7}$$

$$\mathbf{b} \;=\; \mathbf{r}_b \,-\, \mathbf{r}_i \tag{8}$$

The unit-strength velocity vector $\hat{\mathbf{v}}_i$ depends only on the relative positions $\mathbf{a}$, $\mathbf{b}$ between the vortex endpoints and control point.

3.3 Velocity field of source and doublet line segment

The volume contribution to the induced velocity is determined via the source/length density σ and doublet/length density $\boldsymbol{\nu}$ whick model the body. Both are set to give flow tangency on the circular body of cross-sectional area πR^2, immersed in the local apparent-freestream velocity vector, as shown in Figure 3.3.

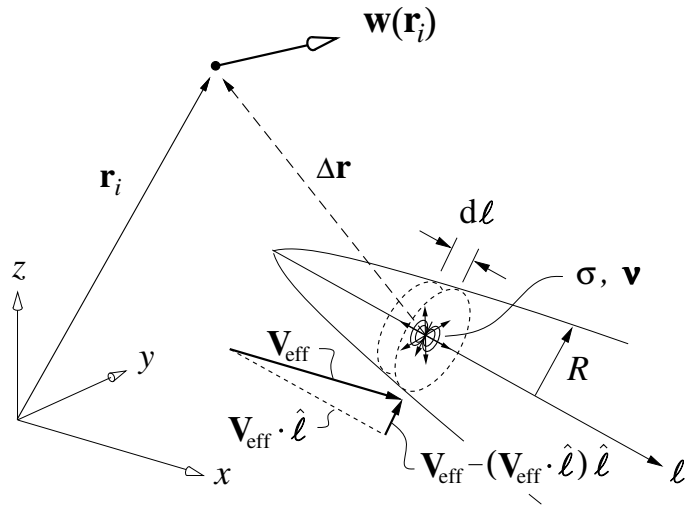

Figure 5: Induced velocity contributions from source and doublet strengths representing a slender body of local radius $R(\ell)$.

$$\mathbf{V}_{\text{eff}} \;=\; \mathbf{V} \,-\, \boldsymbol{\Omega}\times\mathbf{r} \tag{9}$$

$$\sigma(\ell) \;=\; \frac{d(\pi R^2)}{d\ell}\,\Big(\mathbf{V}_{\text{eff}}\cdot\hat{\boldsymbol{\ell}}\Big) \tag{10}$$

$$\boldsymbol{\nu}(\ell) \;=\; 2\,\pi R^2\Big(\mathbf{V}_{\text{eff}} - (\mathbf{V}_{\text{eff}}\cdot\hat{\boldsymbol{\ell}})\hat{\boldsymbol{\ell}}\Big) \tag{11}$$

The integrated effects of all the densities then gives the volume influence function in physical space.

$$\mathbf{w}(\mathbf{r}_i) \;\equiv\; \mathbf{w}_i \;=\; \frac{1}{4\pi}\int\left[\frac{\sigma\Delta\mathbf{r}}{(\Delta r^2+\varepsilon^2)^{3/2}} + \frac{\boldsymbol{\nu}\,\Delta r^2 \,-\, 3(\boldsymbol{\nu}\cdot\Delta\mathbf{r})\,\Delta\mathbf{r}}{(\Delta r^2+\varepsilon^2)^{5/2}}\right]\mathrm{d}\ell \tag{12}$$

$$\Delta\mathbf{r}(\ell) \;=\; \mathbf{r}_i \,-\, \mathbf{r}(\ell) \tag{13}$$

A suitable desingularizing "core size" is $\varepsilon = R/2$. Since σ and $\boldsymbol{\nu}$ depend linearly on $\mathbf{V}$ and $\boldsymbol{\Omega}$, as given by (9), (10), (11), the discretized volume-induced velocity integral (12) can be given in the following form.

$$\mathbf{w}_i \;=\; \sum_{k=1}^{3} \hat{\mathbf{w}}^V_{ik} V_k \;+\; \sum_{k=1}^{3} \hat{\mathbf{w}}^\Omega_{ik} \Omega_k \tag{14}$$

The influence-coefficient vectors $\hat{\mathbf{w}}$ can be evaluated a priori from the body geometry, via the discretized integral (12).

With the $\mathbf{v}_i$ and $\mathbf{w}_i$ relations developed above, the total surface-relative velocity expression (4) can be given in the following form.

$$\mathbf{W}_i(\Gamma_j, V_k, \Omega_k) \;=\; \sum_j \hat{\mathbf{v}}_{ij}\, \Gamma_j \;+\; \sum_k \left[\, \hat{\mathbf{e}}_k + \hat{\mathbf{w}}^V_{ik} \right] V_k \;+\; \sum_k \left[-\hat{\mathbf{e}}_k \times \mathbf{r}_i + \hat{\mathbf{w}}^\Omega_{ik} \right] \Omega_k \tag{15}$$

In this approximate treatment, the influence of the horseshoe vortices is not included in $\mathbf{V}_{\text{eff}}$, so that $\mathbf{w}$ has been eliminated by explicitly giving it in terms of $\mathbf{V}$ and $\boldsymbol{\Omega}$. The full treatment would require that the discrete σ and $\boldsymbol{\nu}$ values be solved implicitly together with Γ_j, which is deemed to be an unwarranted complication given the approximations inherent in the simple source/doublet model used for the slender bodies.

3.4 Section lift and drag coefficients

The surface flow tangency equation used in JVL incorporates a flow separation model which depends on the local lift coefficient c_ℓ, defined for a chord section or "strip". The viscous drag model uses a local profile drag coefficient c_d, which is computed from the c_ℓ via a specified profile drag polar. Both models therefore require the local c_ℓ to be defined.

The section circulation around a chord strip is the summation of the horseshoe vortex strengths on that surface chord strip, as shown in Figure 5.1.2.

$$\Gamma \;=\; \sum_{\text{chord}} \Gamma_i \tag{16}$$

The average surface-relative velocity W is obtained from the area-weighted average velocities on all the elements in that chord strip

$$A \;=\; \sum_{\text{chord}} A_i \tag{17}$$

$$W \;=\; \frac{1}{A} \sum_{\text{chord}} A_i\, W_i \tag{18}$$

where A_i is the area of the element containing the i'th vortex segment (see Figure 2.1). The strip lift coefficient is defined as

$$c_\ell \;=\; \frac{2\Gamma}{Wc} \tag{19}$$

where c is the strip chord, and the section drag coefficient can then be obtained from a specified 2D profile drag polar function.

$$c_{d(r)} \;=\; c_d(c_\ell, c_J, c_Q, Ma, Re) \tag{20}$$

$$Ma_{(r)} \;=\; W/a \tag{21}$$

$$Re_{(r)} \;=\; \rho W c/\mu \tag{22}$$

The local jet momentum and mass coefficients c_J and c_Q will be considered later.

It should also be noted that the c_ℓ and c_d coefficients considered here do *not* include the jet thrust force, which is accounted for separately in the overall force calculation. Their main purpose is to allow modeling of profile drag and any viscous separation effects which might be present.

4 System Solution

4.1 Normal vector

The normal vector at control point i is defined as

$$\hat{\mathbf{n}}_i(\mathcal{D}_l) = \hat{\mathbf{n}}_i^o + \sum_l \hat{\mathbf{n}}_{il}^{\mathcal{D}} \mathcal{D}_l \tag{23}$$

$$\hat{\mathbf{n}}_{il}^{\mathcal{D}} = \hat{\mathbf{h}}_l \times \hat{\mathbf{n}}_i^o \tag{24}$$

where $\hat{\mathbf{n}}_i^o$ is the normal vector of the baseline geometry. The summation term represents a small control surface deflection, where each control variable $\mathcal{D}_l$ effectively rotates the normal vector about the hinge-axis unit vector $\hat{\mathbf{h}}_l$, via the corresponding gain $\hat{\mathbf{n}}_{il}^{\mathcal{D}}$.

4.2 Flow tangency

The flow-tangency equation at each surface control point is

$$\mathbf{W}_i \cdot \hat{\mathbf{n}}_i = W_{n_i} \tag{25}$$

$$W_{n_i}(\Gamma_j, V_k, \Omega_k) = W\, f_{\text{stall}(c_\ell)}\, 2\xi_i^2 \tag{26}$$

where W_{n_i} is a "surface leakage" velocity which is defined to be nonzero only if separation is present, and thus models the resulting loss of lift as shown in Figure 4.2. The ξ quantity in (26) is the fractional chordwise distance. The $2\xi_i^2$ factor concentrates most of the leakage effect near the trailing edge, and thus mimics actual separation progression of trailing-edge type stall. Leading edge stall could be crudely modeled with an alternative chordwise-constant factor. The overall

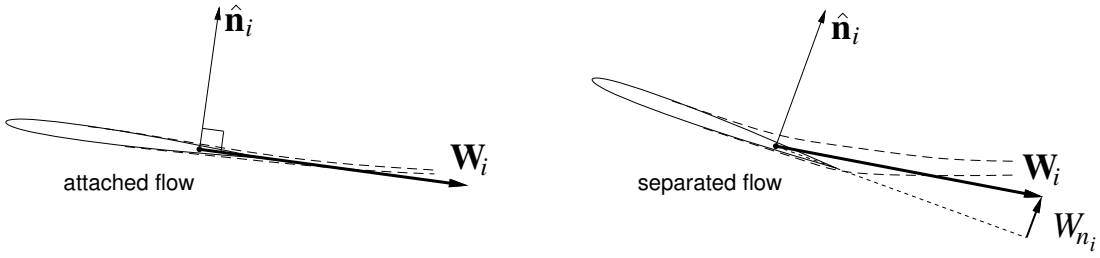

Figure 6: "Leakage" velocity W_n introduced to model flow separation.

degree of leakage is controlled by the $f_{\text{stall}(c_\ell)}$ function, which is constructed to be zero over the unstalled region, and increase rapidly as a stall limit is exceeded. A suitable definition is

$$f_{\text{stall}(c_\ell)} = \frac{K_s}{2\pi}\, \Delta c_\ell\, \log \frac{1 + \exp[(c_\ell - c_{\ell_{\max}})/\Delta c_\ell]}{1 + \exp[(c_{\ell_{\min}} - c_\ell)/\Delta c_\ell]} \tag{27}$$

$$K_s \simeq 40$$

The resulting section lift-curve slope is approximately

$$\frac{\mathrm{d}c_\ell}{\mathrm{d}\alpha} \;\simeq\; \frac{2\pi}{1 + f'_{\mathrm{stall}}} \tag{28}$$

giving the $c_\ell(\alpha)$ curve sketched in Figure 4.2.

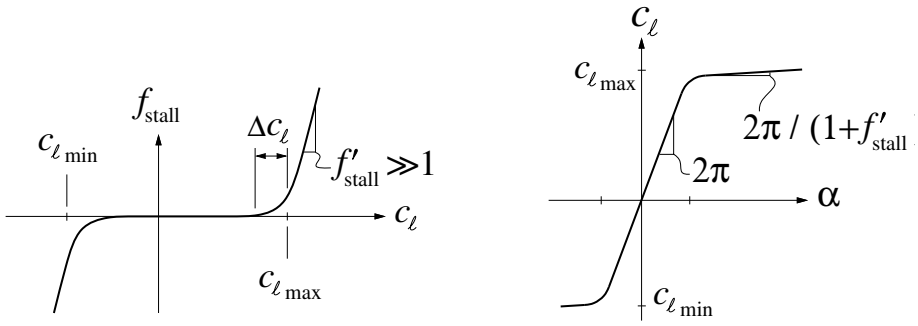

Figure 7: Stall function, active only outside of the stall limits, and resulting $c_\ell(\alpha)$ curve.

4.3 Jet sheet curvature/loading relation

The effects of the jet sheet on the potential flow have been examined by Maskell and Spence [3]. The normal-momentum equation for a curved jet, together with the requirement of continuous static pressure across the jet, gives the following relation between the jet momentum excess per span $\Delta J'$, flow curvature κ, and net vortex sheet strength γ_w.

$$\rho W \gamma_w \;=\; \Delta J' \, \kappa \tag{29}$$

$$\Delta J' \;\equiv\; \int \left(\rho_{\mathrm{jet}} u_{\mathrm{jet}}^2 - \rho W^2 \right) \, \mathrm{d}n \tag{30}$$

$$\;=\; J' \;-\; \rho W^2 \, h_{\mathrm{jet}} \;\simeq\; J' \;-\; \rho V^2 \, h_{\mathrm{jet}} \tag{31}$$

Here, $W = |\mathbf{W}|$ is the local total velocity magnitude averaged between the two sides of the sheet, and will be approximated as equal to the freestream speed V, which is reasonable in the wake. The integration over $\mathrm{d}n$ is across the thickness of the jet sheet. The nonzero vortex sheet strength of the jet adds to the circulation about the physical chord, and reflects most of the lift added by the jet. The detailed force accounting will be done in a later section.

4.4 Discrete equation system

4.4.1 Surface flow tangency

The flow-tangency equation (25) at each surface control point, put into residual form, is

$$R_i(\Gamma_j, V_k, \Omega_k, \mathcal{D}_l) \;\equiv\; \mathbf{W}_i \cdot \hat{\mathbf{n}}_i \;-\; W_{n_i} \;=\; 0 \tag{32}$$

which is then expanded as follows using the vortex-lattice velocity expression (15) for $\mathbf{W}_i$.

$$R_i \;\equiv\; \sum_j A_{ij} \, \Gamma_j \;+\; \sum_k a^V_{ik} \, V_k \;+\; \sum_k a^\Omega_{ik} \, \Omega_k \;+\; \sum_l a^{\mathcal{D}}_{il} \, \mathcal{D}_l \;-\; W_{n_i} \tag{33}$$

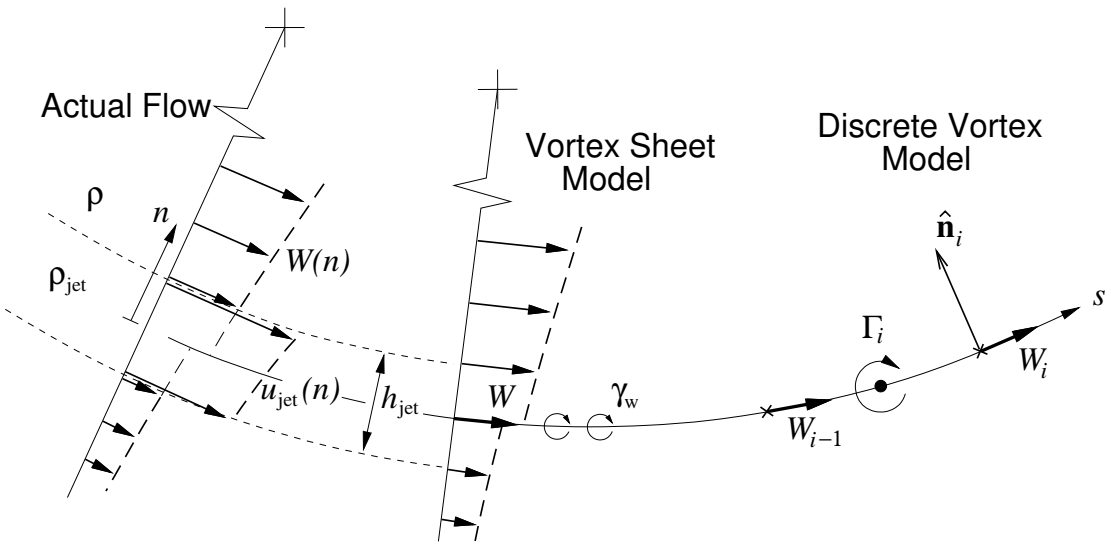

Figure 8: Jet sheet results in net vortex sheet strength γ_w.

$$
\begin{aligned}
A_{ij} &= \hat{\mathbf{v}}_{ij} \cdot \hat{\mathbf{n}}_i^o && (34)\\
a_{ik}^V &= \hat{\mathbf{e}}_k \cdot \hat{\mathbf{n}}_i^o && (35)\\
a_{ik}^\Omega &= -(\hat{\mathbf{e}}_k \times \mathbf{r}_i) \cdot \hat{\mathbf{n}}_i^o && (36)\\
a_{il}^{\mathcal{D}}(\Gamma_j, V_k, \Omega_k) &= \mathbf{W}_i \cdot \hat{\mathbf{n}}_{il}^{\mathcal{D}} \;\simeq\; (\mathbf{V} - \boldsymbol{\Omega} \times \mathbf{r}_i) \cdot \hat{\mathbf{n}}_{il}^{\mathcal{D}} && (37)\\
W_{n_i}(\Gamma_j, V_k, \Omega_k) &= W\, f_{\mathrm{stall}(c_\ell)}\, 2(x/c)_i^2 && (38)
\end{aligned}
$$

The approximation in (37) assumes that the control-deflection influence vectors $\hat{\mathbf{n}}_{il}^{\mathcal{D}}$ are mostly chordwise and hence mostly perpendicular to the induced velocity $\mathbf{v}_i$, so that $\mathbf{v}_i \cdot \hat{\mathbf{n}}_{il}^{\mathcal{D}}$ can be dropped from $\mathbf{W}_i$. The simplification is significant in that it makes R_i depend strictly linearly on Γ_j, provided $W_{n_i} = 0$ with no separation present.

4.4.2 Jet sheet curvature

The discrete form of the jet sheet curvature equation (29) is obtained by integrating it in the streamwise direction between two control points at $i-1$ and i, straddling a bound vortex segment of strength Γ_i replacing the distributed sheet strength γ_w, as shown in Figure 4.3.

$$
\begin{aligned}
\rho V \int_{s_{i-1}}^{s_i} \gamma_w \, \mathrm{d}s &= \Delta J' \int_{s_{i-1}}^{s_i} \kappa \, \mathrm{d}s && (39)\\
\rho V \Gamma_i &= \Delta J' \, (\theta_i - \theta_{i-1}) && (40)\\
\rho V^2 \Gamma_i &= \Delta J' \, (\mathbf{W}_i - \mathbf{W}_{i-1}) \cdot \hat{\mathbf{n}}_i && (41)
\end{aligned}
$$

The last equation assumes that the change in the streamline angle θ is small between the two points. This finally gives the following residual, which is applied to each jet sheet control point i, in lieu of the solid-surface residual (32).

$$
\begin{aligned}
R_i(\Gamma_j, V_k, \Omega_k, \mathcal{P}_l) &\equiv \bar{J}_i \, (\mathbf{W}_i - \mathbf{W}_{i-1}) \cdot \hat{\mathbf{n}}_i \;-\; \Gamma_i \;=\; 0 && (42)\\
\bar{J}_i &\equiv \frac{\Delta J'}{\rho V^2} \;=\; \int \left(\frac{\rho_{\mathrm{jet}} u_{\mathrm{jet}}^2}{\rho V^2} - 1 \right) \mathrm{d}n && (43)
\end{aligned}
$$

Note that the normalized jet momentum excess $\bar{J}_i$ has the units of length, and in practice will typically scale with the local chord.

For computational purposes, each $\bar{J}_i$ is defined as the sum of any number of terms,

$$\bar{J}_i(\mathcal{P}_l) \;=\; \sum_l a_{il}^{\mathcal{P}} \mathcal{P}_l \tag{44}$$

with the terms giving the contributions of global $\mathcal{P}_l$ variables, each possibly representing a throttle setting or differential throttle setting. The local weighting factor $a_{il}^{\mathcal{P}}$ has the same value all along a chordwise strip of the wake, but can of course vary from strip to strip. The residual (42) is expanded as follows using the vortex-lattice velocity expression (15) for $\mathbf{W}_i$.

$$R_i \;\equiv\; \sum_j B_{ij}\,\Gamma_j \;+\; \sum_k b_{ik}^{\Omega}\,\Omega_k \tag{45}$$

$$B_{ij}(\mathcal{P}_l) \;=\; \begin{cases} \bar{J}_i\,(\hat{\mathbf{v}}_{ij} - \hat{\mathbf{v}}_{i-1j}) \cdot \hat{\mathbf{n}}_i^o & , \quad j \neq i \\ \bar{J}_i\,(\hat{\mathbf{v}}_{ij} - \hat{\mathbf{v}}_{i-1j}) \cdot \hat{\mathbf{n}}_i^o \;-\; 1 & , \quad j = i \end{cases} \tag{46}$$

$$b_{ik}^{\Omega}(\mathcal{P}_l) \;=\; -\bar{J}_i\,\hat{\mathbf{e}}_k \times (\mathbf{r}_i - \mathbf{r}_{i-1}) \cdot \hat{\mathbf{n}}_i^o \tag{47}$$

4.4.3 Global equations

The residual equations constraining the global variables have the form

$$R_V(\Gamma_j, V_k, \Omega_k, \mathcal{D}_l, \mathcal{P}_l) \;=\; 0 \tag{48}$$

$$R_\Omega(\Gamma_j, V_k, \Omega_k, \mathcal{D}_l, \mathcal{P}_l) \;=\; 0 \tag{49}$$

$$R_{\mathcal{D}}(\Gamma_j, V_k, \Omega_k, \mathcal{D}_l, \mathcal{P}_l) \;=\; 0 \tag{50}$$

$$R_{\mathcal{P}}(\Gamma_j, V_k, \Omega_k, \mathcal{D}_l, \mathcal{P}_l) \;=\; 0 \tag{51}$$

where the $R_V \ldots R_{\mathcal{P}}$ functions can be direct constraints on the variables, e.g.

$$R_V(V_k) \;\equiv\; V_k \;-\; V_{k_{\rm spec}} \tag{52}$$

or indirect constraints on the force or moment, e.g.

$$R_V(\Gamma_j, V_k, \Omega_k, \mathcal{P}_l) \;\equiv\; \mathbf{F}(\Gamma_j, V_k, \Omega_k, \mathcal{P}_l) \;-\; \mathbf{F}_{\rm spec} \tag{53}$$

The force function $\mathbf{F}$ is obtained by direct force calculation with the vortex lattice solution, or from the Trefftz Plane, as described later.

4.5 Newton linearization

To drive each residual to zero, we impose the linearized approximation $\delta R_i + R_i = 0$. For the solid-surface residual (33) this has the following form.

$$\frac{\partial R_i}{\partial \Gamma_j}\,\delta\Gamma_j \;+\; \frac{\partial R_i}{\partial V_k}\,\delta V_k \;+\; \frac{\partial R_i}{\partial \Omega_k}\,\delta\Omega_k \;+\; \frac{\partial R_i}{\partial \mathcal{D}_l}\,\delta\mathcal{D}_l \;+\; \frac{\partial R_i}{\partial \mathcal{P}_l}\,\delta\mathcal{P}_l \;+\; R_i \;=\; 0 \tag{54}$$

For a solid surface point, the Jacobian elements have the following form.

$$\frac{\partial R_i}{\partial \Gamma_j} \;=\; A_{ij} \;-\; \frac{\partial W_{n_i}}{\partial \Gamma_j} \tag{55}$$

$$\frac{\partial R_i}{\partial V_k} = a_{ik}^V - \frac{\partial W_{n_i}}{\partial V_k} \tag{56}$$

$$\frac{\partial R_i}{\partial \Omega_k} = a_{ik}^\Omega - \frac{\partial W_{n_i}}{\partial \Omega_k} \tag{57}$$

$$\frac{\partial R_i}{\partial \mathcal{D}_l} = a_{il}^\mathcal{D} \tag{58}$$

$$\frac{\partial R_i}{\partial \mathcal{P}_l} = 0 \tag{59}$$

For a jet sheet point, they have the following form.

$$\frac{\partial R_i}{\partial \Gamma_j} = B_{ij} \tag{60}$$

$$\frac{\partial R_i}{\partial V_k} = 0 \tag{61}$$

$$\frac{\partial R_i}{\partial \Omega_k} = b_{ik}^\Omega \tag{62}$$

$$\frac{\partial R_i}{\partial \mathcal{D}_l} = 0 \tag{63}$$

$$\frac{\partial R_i}{\partial \mathcal{P}_l} = b_{il}^\mathcal{P} = a_{il}^\mathcal{P} \left(\mathbf{W}_i - \mathbf{W}_{i-1}\right) \cdot \hat{\mathbf{n}}_i \tag{64}$$

The linearizations of the remaining global-variable residuals have the form

$$\frac{\partial R_V}{\partial \Gamma_j}\,\delta\Gamma_j + \frac{\partial R_V}{\partial V_k}\,\delta V_k + \frac{\partial R_V}{\partial \Omega_k}\,\delta\Omega_k + \frac{\partial R_V}{\partial \mathcal{D}_l}\,\delta\mathcal{D}_l + \frac{\partial R_V}{\partial \mathcal{P}_l}\,\delta\mathcal{P}_l + R_V = 0 \tag{65}$$

where the partial derivatives are evaluated at the current iteration level.

4.6 Newton system structure

The overall Newton linear system which is solved every iteration is assembled and partitioned as follows.

$$\begin{array}{|c|c|c|c|c|}
\hline
\frac{\partial R_i}{\partial \Gamma_j} & \frac{\partial R_i}{\partial V_k} & \frac{\partial R_i}{\partial \Omega_k} & \frac{\partial R_i}{\partial \mathcal{D}_l} & \frac{\partial R_i}{\partial \mathcal{P}_l} \\
\hline
\frac{\partial R_V}{\partial \Gamma_j} & \frac{\partial R_V}{\partial V_k} & \frac{\partial R_V}{\partial \Omega_k} & \frac{\partial R_V}{\partial \mathcal{D}_l} & \frac{\partial R_V}{\partial \mathcal{P}_l} \\
\hline
\frac{\partial R_\Omega}{\partial \Gamma_j} & \frac{\partial R_\Omega}{\partial V_k} & \frac{\partial R_\Omega}{\partial \Omega_k} & \frac{\partial R_\Omega}{\partial \mathcal{D}_l} & \frac{\partial R_\Omega}{\partial \mathcal{P}_l} \\
\hline
\frac{\partial R_\mathcal{D}}{\partial \Gamma_j} & \frac{\partial R_\mathcal{D}}{\partial V_k} & \frac{\partial R_\mathcal{D}}{\partial \Omega_k} & \frac{\partial R_\mathcal{D}}{\partial \mathcal{D}_l} & \frac{\partial R_\mathcal{D}}{\partial \mathcal{P}_l} \\
\hline
\frac{\partial R_\mathcal{P}}{\partial \Gamma_j} & \frac{\partial R_\mathcal{P}}{\partial V_k} & \frac{\partial R_\mathcal{P}}{\partial \Omega_k} & \frac{\partial R_\mathcal{P}}{\partial \mathcal{D}_l} & \frac{\partial R_\mathcal{P}}{\partial \mathcal{P}_l} \\
\hline
\end{array}
\begin{array}{|c|}
\hline
\delta\Gamma_j \\
\hline
\delta V_k \\
\hline
\delta\Omega_k \\
\hline
\delta\mathcal{D}_l \\
\hline
\delta\mathcal{P}_l \\
\hline
\end{array}
+
\begin{array}{|c|}
\hline
R_i \\
\hline
R_V \\
\hline
R_\Omega \\
\hline
R_\mathcal{D} \\
\hline
R_\mathcal{P} \\
\hline
\end{array}
= 0 \tag{66}$$

4.7 Newton system solution

The solution of the overall Newton system (66) above begins by premultiplying the top row block by $[\partial R_i/\partial\Gamma_j]^{-1}$ via back-substitution of the $\partial R_i/\partial V \ldots$ vectors into the LU-factored $[\partial R_i/\partial\Gamma_j]$ matrix.

$$\delta\Gamma_i \;+\; c^V_{ik}\,\delta V_k \;+\; c^\Omega_{ik}\,\delta\Omega_k \;+\; c^\mathcal{D}_{il}\,\delta\mathcal{D}_l \;+\; c^\mathcal{P}_{il}\,\delta\mathcal{P}_l \;+\; R'_i \;=\; 0 \tag{67}$$

where

$$c^V_{ik} \;=\; \left[\frac{\partial R_i}{\partial\Gamma_j}\right]^{-1}\left\{\frac{\partial R_i}{\partial V_k}\right\} \tag{68}$$

$$\vdots$$

Equation (67) is then used to eliminate the $\delta\Gamma_j$ column from the remaining rows of the Newton system (66), giving a small square matrix equation for the global variables $\delta V_k \ldots \delta\mathcal{P}_l$. These are then used in (67) to obtain the final $\delta\Gamma_i$ values.

The solution to the Newton system is then used to update all the unknowns.

$$\Gamma_i \;\leftarrow\; \Gamma_i \;+\; \delta\Gamma_i \tag{69}$$
$$V_k \;\leftarrow\; V_k \;+\; \delta V_k \tag{70}$$
$$\Omega_k \;\leftarrow\; \Omega_k \;+\; \delta\Omega_k \tag{71}$$
$$\mathcal{D}_l \;\leftarrow\; \mathcal{D}_l \;+\; \delta\mathcal{D}_l \tag{72}$$
$$\mathcal{P}_l \;\leftarrow\; \mathcal{P}_l \;+\; \delta\mathcal{P}_l \tag{73}$$

These new values are then used to recompute the matrix of the Newton system (66) at the start of the next iteration.

4.8 Factored matrix re-use

It is useful to note that if the following conditions hold:

- there is no viscous separation modeling, i.e. $W_{n_i}=0$ everywhere, and
- there is no jet flow, i.e. $\bar{J}_i=0$ everywhere,

then $\partial R_i/\partial\Gamma_j = A_{ij}$ is independent of the state variables. In this case, the factorization needed for $[\partial R_i/\partial\Gamma_j]^{-1}$ needs to be performed only once for any given geometry, giving considerable computational savings for all Newton iterations after the first one, especially when multiple operating points need to be computed.

5 Force calculation

The overall force on the configuration will be computed in two ways: 1) a near-field force and jet momentum summation over the configuration, and 2) a far-field momentum summation over the trailing vortex and jet sheets in the Trefftz-Plane. For the overall moment, only the near-field approach is suitable.

For both the near-field and far-field approaches, three separate contributions are considered:

$$\mathbf{F} \;=\; \mathbf{F}_{\text{inv}} \;+\; \mathbf{F}_{\text{jet}} \;+\; \mathbf{F}_{\text{vis}} \tag{74}$$
$$\mathbf{F}^{\text{TP}} \;=\; \mathbf{F}^{\text{TP}}_{\text{inv}} \;+\; \mathbf{F}^{\text{TP}}_{\text{jet}} \;+\; \mathbf{F}^{\text{TP}}_{\text{vis}} \tag{75}$$

An explicit expression for each term will now be derived.

5.1 Nearfield forces

5.1.1 Velocities on vortex segments

The total surface-relative velocity at a vortex-segment midpoint $\mathbf{r}'_i$ is given by equation (15),

$$\mathbf{W}'_i = \mathbf{v}'_i + \mathbf{w}'_i + \mathbf{V} - \mathbf{\Omega} \times \mathbf{r}'_i \tag{76}$$

$$\mathbf{v}'_i = \sum_j \hat{\mathbf{v}}'_{ij}\, \Gamma_j \tag{77}$$

$$\mathbf{w}'_i = \sum_k \hat{\mathbf{w}}'^{V}_{ik}\, V_k + \sum_k \hat{\mathbf{w}}'^{\Omega}_{ik}\, \Omega_k \tag{78}$$

where j is the dummy summation index over all horseshoe vortices. Each influence coefficient $\hat{\mathbf{v}}'_{ij}$ excludes the singular self-influence of its own bound vortex segment in the integration, in contrast to the $\hat{\mathbf{v}}_{ij}$ located at the control point which does include the bound vortex contribution.

5.1.2 Inviscid force and moment

Figure 5.1.2 shows the velocity on vortex segment i. The resulting inviscid force on the segment is

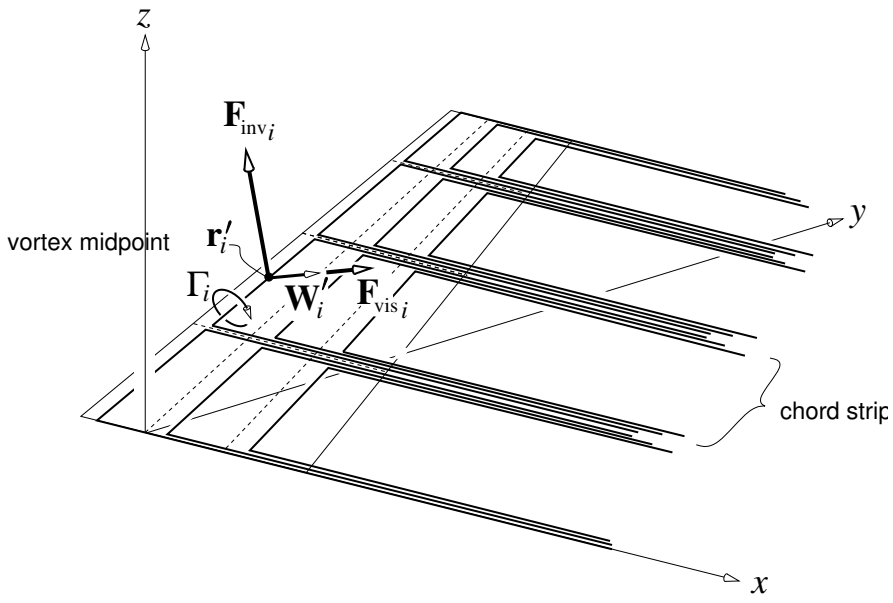

Figure 9: Circulation Γ_i, relative velocity $\mathbf{W}'_i$, and resulting forces $\mathbf{F}_{\mathrm{inv}_i}$,$\mathbf{F}_{\mathrm{vis}_i}$ on vortex segment, perpendicular and parallel to $\mathbf{W}'_i$.

computed using the Kutta-Joukowsky relation.

$$\mathbf{F}_{\mathrm{inv}_i} = \rho \Gamma_i\, \mathbf{W}'_i \times \boldsymbol{\ell}_i \qquad \text{(bound vortex)} \tag{79}$$

where $\boldsymbol{\ell}_i$ is the segment length vector in the positive Γ_i direction. For a slender body, the force on a segment $\boldsymbol{\ell}_i$ of the body is calculated as follows.

$$\mathbf{F}_{\mathrm{inv}_i} = \rho \sigma \ell_i \left[\mathbf{V}_{\mathrm{eff}} - \left(\mathbf{V}_{\mathrm{eff}} \cdot \hat{\boldsymbol{\ell}}_i \right) \hat{\boldsymbol{\ell}}_i \right] \qquad \text{(slender body)} \tag{80}$$

The total force and moment are the summations over all segments on all surfaces and bodies.

$$\mathbf{F}_{\text{inv}} = \sum_i \mathbf{F}_{\text{inv}_i} \tag{81}$$

$$\mathbf{M}_{\text{inv}} = \sum_i \mathbf{r}'_i \times \mathbf{F}_{\text{inv}_i} \tag{82}$$

5.1.3 Jet force and moment

The local jet velocity and mass flow per span are first determined from the local $\bar{J}$, and a specified jet height h_{jet} and jet density ratio ρ_{jet}/ρ.

$$\frac{J'}{\rho V^2} = \bar{J} + h_{\text{jet}} \tag{83}$$

$$\frac{u_{\text{jet}}}{V} = \sqrt{\frac{\rho}{\rho_{\text{jet}}} \frac{1}{h_{\text{jet}}} \frac{J'}{\rho V^2}} = \sqrt{\frac{\rho}{\rho_{\text{jet}}} \left(\frac{\bar{J}}{h_{\text{jet}}} + 1 \right)} \tag{84}$$

$$\frac{\dot{m}'}{\rho V} = \frac{\rho_{\text{jet}}}{\rho} \frac{u_{\text{jet}}}{V} h_{\text{jet}} = \sqrt{\frac{\rho_{\text{jet}}}{\rho} h_{\text{jet}} \left(\bar{J} + h_{\text{jet}} \right)} \tag{85}$$

The jet sheet flow is assumed to issue from the exhaust nozzle along some direction given by the vector $\mathbf{T}_0$ (magnitude not significant). The trailing edge flap is then assumed to turn only the component of $\mathbf{T}_0$ which is along the trailing edge normal vector, with the remaining component left unaffected. The unit direction vector $\hat{\mathbf{T}}$ of the turned jet is then computed as follows, for each trailing edge point.

$$\hat{\mathbf{T}}_i = \frac{\mathbf{T}_{0_i} - (\mathbf{T}_{0_i} \cdot \hat{\mathbf{n}}_i)\, \hat{\mathbf{n}}_i}{|\mathbf{T}_{0_i} - (\mathbf{T}_{0_i} \cdot \hat{\mathbf{n}}_i)\, \hat{\mathbf{n}}_i|} \quad , \quad i \in i_{TE} \tag{86}$$

The net strip jet force is then given by the momentum flow change from the freestream direction,

$$\mathbf{F}_{\text{jet}_i} = -\left(J'_i \hat{\mathbf{T}}_i - \dot{m}'_i \mathbf{V} \right) \ell_i \quad , \quad i \in i_{TE} \tag{87}$$

$$\ell_i = |\hat{\mathbf{x}} \times \boldsymbol{\ell}_i| \tag{88}$$

where ℓ_i is the width of the chord strip. Since $\hat{\mathbf{n}}_{i_{TE}}$ depends on the flap deflection variables $\mathcal{D}_l$ via its definition (23), then $\hat{\mathbf{T}}_i$ and hence $\mathbf{F}_{\text{jet}_i}$ depend on $\mathcal{D}_l$ as well. This captures the thrust-vectoring effect of the blown jet flap.

The jet sheet is assumed to apply a point load at the trailing edge location $\mathbf{r}_{i_{TE}}$ at each surface strip. These are summed over all strip trailing edge points to obtain the overall jet force and moment.

$$\mathbf{F}_{\text{jet}} = \sum_{i \in i_{TE}} \mathbf{F}_{\text{jet}_i} \tag{89}$$

$$\mathbf{M}_{\text{jet}} = \sum_{i \in i_{TE}} \mathbf{r}_i \times \mathbf{F}_{\text{jet}_i} \tag{90}$$

It is also convenient at this point to compute the total momentum and mass flows for the entire configuration, by summing over the chord strips.

$$J = \sum_{i \in i_{TE}} J'_i \, \ell_{TE} \tag{91}$$

$$\dot{m} = \sum_{i \in i_{TE}} \dot{m}'_i \, \ell_{TE} \tag{92}$$

5.1.4 Viscous force and moment

The viscous force of each panel is computed using the chord strip drag coefficient defined by (20).

$$\mathbf{F}_{\mathrm{vis}_i} = \frac{1}{2}\rho W \mathbf{W}'_i \, c_d \, A_i \tag{93}$$

Note that the profile drag is distributed over the chord strip, and acts along the local total relative velocity $\mathbf{W}$, as shown in Figure 5.1.2. Finally, the viscous force and moment contributions are obtained by summing over all vortex segments for all the surfaces.

$$\mathbf{F}_{\mathrm{vis}} = \sum_i \mathbf{F}_{\mathrm{vis}_i} \tag{94}$$

$$\mathbf{M}_{\mathrm{vis}} = \sum_i \mathbf{r}_i \times \mathbf{F}_{\mathrm{vis}_i} \tag{95}$$

5.1.5 Body force and moment

The forces on a body are computed using slender-body theory.

$$\mathbf{F}_{\mathrm{body}_i} = \rho\sigma_i \left(\mathbf{V}_{\mathrm{eff}} - (\mathbf{V}_{\mathrm{eff}} \cdot \hat{\boldsymbol{\ell}})\,\hat{\boldsymbol{\ell}}\right)_i \ell_i \tag{96}$$

$$\mathbf{F}_{\mathrm{body}} = \sum_i \mathbf{F}_{\mathrm{body}_i} \tag{97}$$

$$\mathbf{M}_{\mathrm{body}} = \sum_i \mathbf{r}'_i \times \mathbf{F}_{\mathrm{body}_i} \tag{98}$$

The local force acts perpendicular to the body centerline. It's also useful to note that for a closed body the summed source strength vanishes, $\sum \sigma_i \ell_i = 0$, so that $\mathbf{F}_{\mathrm{body}} \simeq 0$ is expected. However, the moment $\mathbf{M}_{\mathrm{body}} \neq 0$, and this method predicts the destabilizing pitch and yaw moments characteristic of slender bodies.

5.2 Farfield (Trefftz Plane) forces

An alternative method of computing the overall forces is via the Trefftz Plane. This is a far-field approach which does not suffer from from the massive force cancellation and consequent loss of accuracy which is typical in near-field surface force summation.

5.2.1 Trefftz Plane configuration

The Trefftz Plane is the y-z plane behind the configuration, which is pierced by the trailing vortex sheets, as shown in Figure 5.2.1. The vortex sheets carry the discrete trailing legs of the horseshoe vortices, and also the mass and momentum flow of any jet sheets present. In reality, the trailing vorticity is aligned with the local velocity. However, the computational model assumes that the vortices lie in the fixed $\hat{\mathbf{x}}$ direction, parallel to the x axis.

The circulation of each trailing leg bundle pair in the vortex sheet is the total circulation Γ_{strip} of the horseshoe vortices in that strip, including ones on the jet sheet.

$$\Gamma_l = \pm\Gamma_{\mathrm{strip}} \tag{99}$$

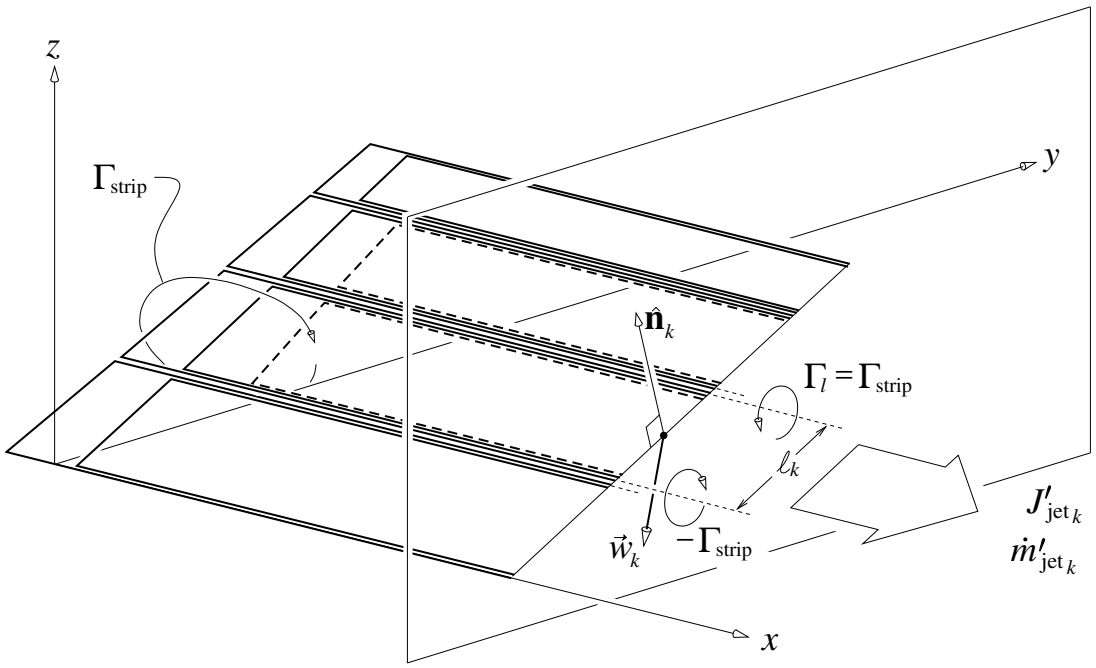

Figure 10: Trefftz Plane with trailing vortices, and jet sheet mass and momentum flows per span.

This differs from the section circulation Γ definition (16), which does not include the jet sheet vortices. All the $\pm\Gamma_l$ circulation pairs induce a velocity $\mathbf{w}_k$ at each strip midpoint.

$$\mathbf{w}_k = \frac{1}{2\pi} \sum_l \Gamma_l \left[\frac{\hat{\mathbf{x}} \times (\mathbf{r}_k - \mathbf{r}_l)}{|\mathbf{r}_k - \mathbf{r}_l|^2} - \frac{\hat{\mathbf{x}} \times (\mathbf{r}_k - \mathbf{r}_{l-1})}{|\mathbf{r}_k - \mathbf{r}_{l-1}|^2} \right] \tag{100}$$

By construction, this $\mathbf{w}_k$ lies in the y-z Trefftz Plane.

The jet sheet mass and momentum flows are assumed to be preserved from their strip values at the wing.

$$\dot{m}'_k = (\dot{m}')_{\text{strip}} \tag{101}$$

$$J'_k = (J')_{\text{strip}} \tag{102}$$

5.2.2 Trefftz Plane inviscid force

The inviscid circulation-related lift and sideforce are obtained by a Kelvin impulse integral over the vortex sheet.

$$L^{\text{TP}}_{\text{inv}} = \sum_k \rho V \, \hat{\mathbf{z}} \cdot \hat{\mathbf{n}}_k \, \Gamma_k \, \ell_k \tag{103}$$

$$Y^{\text{TP}}_{\text{inv}} = \sum_k \rho V \, \hat{\mathbf{y}} \cdot \hat{\mathbf{n}}_k \, \Gamma_k \, \ell_k \tag{104}$$

The remaining vortex drag component is obtained by a kinetic energy integral over the vortex sheet.

$$D^{\text{TP}}_{\text{inv}} = \sum_k -\tfrac{1}{2} \rho \, \mathbf{w}_k \cdot \hat{\mathbf{n}}_k \, \Gamma_k \, \ell_k \tag{105}$$

These three force components were computed with the trailing vortices aligned with the x axis. However, a more correct approximation is that they align with the freestream velocity $\mathbf{V}$. Hence, the three force components are now rotated into the wind axes, giving the following total farfield inviscid force vector.

$$\mathbf{F}_{\text{inv}}^{\text{TP}} = D_{\text{inv}}^{\text{TP}}\,\hat{\mathbf{V}} + Y_{\text{inv}}^{\text{TP}}\,\hat{\mathbf{Y}} + L_{\text{inv}}^{\text{TP}}\,\hat{\mathbf{L}} \tag{106}$$

$$\hat{\mathbf{V}} = \mathbf{V}/V \tag{107}$$

$$\hat{\mathbf{Y}} = \hat{\mathbf{z}}\times\hat{\mathbf{V}}\,/\left|\hat{\mathbf{z}}\times\hat{\mathbf{V}}\right| \tag{108}$$

$$\hat{\mathbf{L}} = \hat{\mathbf{V}}\times\hat{\mathbf{Y}} \tag{109}$$

5.2.3 Trefftz Plane jet force

The jet sheet flow in the trailing sheet is assumed to be aligned with the local total velocity, which is the vector sum of $\mathbf{V}$ and $\mathbf{w}_k$. As with the inviscid forces above, we compute the jet force components by working in the xyz axes, in which $\mathbf{w}_k$ was computed. In these axes, the jet sheet momentum is along the unit vector given by

$$\hat{\mathbf{T}}_k = \frac{V\hat{\mathbf{x}} + \mathbf{w}_k}{|V\hat{\mathbf{x}} + \mathbf{w}_k|} = \frac{1}{\sqrt{1+(w_k/V)^2}}\,\hat{\mathbf{x}} + \frac{\mathbf{w}_k/V}{\sqrt{1+(w_k/V)^2}} \tag{110}$$

where $w_k \equiv |\mathbf{w}_k|$, and the alternative second form uses the fact that $\mathbf{w}_k$ as computed via (100) is orthogonal to $\hat{\mathbf{x}}$. The Trefftz-Plane jet force components are then obtained as the momentum changes of the jet mass flow, summed over all the strips.

$$D_{\text{jet}}^{\text{TP}} = \sum_k \left(-J_k'\hat{\mathbf{T}}_k\cdot\hat{\mathbf{x}} + \dot{m}_k' V\right)\ell_k \simeq \sum_k \left(-J_k' + \dot{m}_k' V\right)\ell_k \tag{111}$$

$$Y_{\text{jet}}^{\text{TP}} = \sum_k -J_k'\hat{\mathbf{T}}_k\cdot\hat{\mathbf{y}}\;\ell_k \simeq \sum_k \left(-J_k'\,\mathbf{w}_k\cdot\hat{\mathbf{y}}/V\right)\ell_k \tag{112}$$

$$L_{\text{jet}}^{\text{TP}} = \sum_k -J_k'\hat{\mathbf{T}}_k\cdot\hat{\mathbf{z}}\;\ell_k \simeq \sum_k \left(-J_k'\,\mathbf{w}_k\cdot\hat{\mathbf{z}}/V\right)\ell_k \tag{113}$$

The second approximate forms assume that $w_k/V \ll 1$, although there's little reason to use them in actual computations. Rotating the force components into the wind axes gives the actual farfield jet force vector.

$$\mathbf{F}_{\text{jet}}^{\text{TP}} = D_{\text{inv}}^{\text{TP}}\,\hat{\mathbf{V}} + Y_{\text{inv}}^{\text{TP}}\,\hat{\mathbf{Y}} + L_{\text{inv}}^{\text{TP}}\,\hat{\mathbf{L}} \tag{114}$$

5.2.4 Trefftz Plane viscous force

The farfield viscous force of each strip is its momentum defect, conveniently computed using the profile drag coefficient c_d defined previously.

$$D_{\text{vis}}^{\text{TP}} = \sum_k \tfrac{1}{2}\rho V^2\,A_k\,c_d \tag{115}$$

The strip reference area A_k is the area of the strip on the lifting surface. The viscous lift and sideforce are assumed to be negligible. The total farfield viscous force vector is then given as follows.

$$\mathbf{F}_{\text{vis}}^{\text{TP}} = D_{\text{vis}}^{\text{TP}}\,\hat{\mathbf{V}} \tag{116}$$

5.3 Near-field and Far-field force comparison

The overall near-field and far-field forces are defined as the overall sums.

$$\mathbf{F} = \mathbf{F}_{\text{inv}} + \mathbf{F}_{\text{jet}} + \mathbf{F}_{\text{vis}} \tag{117}$$

$$\mathbf{F}^{\text{TP}} = \mathbf{F}^{\text{TP}}_{\text{inv}} + \mathbf{F}^{\text{TP}}_{\text{jet}} + \mathbf{F}^{\text{TP}}_{\text{vis}} \tag{118}$$

Theoretically, these two total forces should be equal, although $\mathbf{F}^{\text{TP}}$ is expected to be more accurate, especially its drag component along $\hat{\mathbf{v}}$ which is of great practical importance. However, it should be stressed that the inviscid and jet contributions between the two calculation methods are decidedly not equal. Namely, we expect that

$$\mathbf{F} \simeq \mathbf{F}^{\text{TP}} \tag{119}$$

$$\text{but} \quad \mathbf{F}_{\text{inv}} \neq \mathbf{F}^{\text{TP}}_{\text{inv}} \tag{120}$$

$$\text{and} \quad \mathbf{F}_{\text{jet}} \neq \mathbf{F}^{\text{TP}}_{\text{jet}} \tag{121}$$

The reason is that the jet lift force in the near-field surface calculation, which goes into $\mathbf{F}_{\text{jet}}$, is mostly represented by the circulation of jet's bound vortices, which goes into Γ_k and hence $\mathbf{F}^{\text{TP}}_{\text{inv}}$ in the Trefftz Plane. The lift part of the Trefftz Plane jet force $\mathbf{F}^{\text{TP}}_{\text{jet}}$ is quite small by comparison, and in fact is zero in a 2D case, for which $\mathbf{w}_k = 0$, and hence $\hat{\mathbf{T}}_k = \hat{\mathbf{v}}$ as defined by (110).

5.4 Force and moment coefficients

The freestream dynamic pressure $q = \frac{1}{2}\rho V^2$, and the local chord c or strip area A are used as the reference quantities for defining local section coefficients. The local lift and drag coefficients have been defined previously.

$$c_\ell = \frac{L_{\text{strip}}}{qA} = \frac{2\Gamma}{Wc} \tag{122}$$

$$c_d = \frac{D_{\text{strip}}}{qA} \tag{123}$$

Local jet momentum and mass flow coefficients are defined as follows.

$$c_J = \frac{J'}{\frac{1}{2}\rho V^2 c} = 2\,\frac{\bar{J} + h_{\text{jet}}}{c} \tag{124}$$

$$c_Q = \frac{\dot{m}'}{\rho V c} \tag{125}$$

The total momentum and mass flow coefficients are defined as follows.

$$C_J = \frac{J}{\frac{1}{2}\rho V^2 S} \tag{126}$$

$$C_Q = \frac{\dot{m}}{\rho V S} \tag{127}$$

5.5 Spanwise loading figures of merit

To obtain an aerodynamic figure of merit, one can compare the thrust loss of a wing with the minimum possible value. Using the convenient Trefftz Plane forces, we consider the difference between the actual streamwise force and the ideal thrust force which would be obtained if the propulsive flow were aligned with the freestream. We call this thrust loss a generalized *induced drag*.

$$D_{\rm i}^{\rm TP} \;=\; D_{\rm inv}^{\rm TP} \,+\, D_{\rm jet}^{\rm TP} \,+\, J \,-\, \dot{m}V \tag{128}$$

The profile drag $D_{\rm vis}^{\rm TP}$ is excluded from $D_{\rm i}^{\rm TP}$, so that $D_{\rm i}^{\rm TP}$ becomes the conventional induced drag in the non-powered case. It is also convenient to define the corresponding Trefftz-Plane force coefficients.

$$C_{D_{\rm i}} \;\equiv\; \frac{D_{\rm i}^{\rm TP}}{\frac{1}{2}\rho V^2 S} \tag{129}$$

$$C_L \;\equiv\; \frac{L_{\rm inv}^{\rm TP} + L_{\rm jet}^{\rm TP}}{\frac{1}{2}\rho V^2 S} \tag{130}$$

$$C_Y \;\equiv\; \frac{Y_{\rm inv}^{\rm TP} + Y_{\rm jet}^{\rm TP}}{\frac{1}{2}\rho V^2 S} \tag{131}$$

5.5.1 Classical span efficiency

For a wing with a spanwise-elliptical circulation distribution in the Trefftz Plane, the minimum possible $C_{D_{\rm i}}$ has been derived by Thwaites [4].

$$\Big(C_{D_{\rm i}}\Big)_{\rm min} \;=\; \frac{C_L^2}{\pi AR + 2C_J} \tag{132}$$

$$AR \;\equiv\; \frac{b^2}{S} \tag{133}$$

For the non-powered case, $C_J = 0$, and this $C_{D_{\rm i}}$ reduces to the classical Prandtl result. For the powered case, the physical aspect ratio AR is in effect increased by the amount $2C_J/\pi$.

We now define a *span efficiency* which is the ratio of this minimum induced drag and the actual induced drag.

$$e_{\rm span} \;=\; \frac{C_L^2 + C_Y^2}{\pi AR + 2C_J}\,\frac{1}{C_{D_{\rm i}}} \tag{134}$$

The C_Y^2 term has also been added to make the result independent of rotating the wing about the x-axis. This span efficiency indicates how well the overall circulation on the wing and jet (if any) is distributed along the span. For the case of a planar wing with an elliptical circulation distribution it will approach unity, $e_{\rm span} = 1$, as in the classical case.

5.5.2 Thrust-vectoring benefit

An alternative *thrust-vectoring efficiency* is defined by

$$e_{\rm vector} \;=\; \frac{C_L^2 + C_Y^2}{\pi AR}\,\frac{1}{C_{D_{\rm i}}} \tag{135}$$

and indicates the benefit of combining the propulsive jet with the wing's vortex wake. If an elliptically loaded wing is aerodynamically isolated from the jet, we have $e_{\rm vector} = 1$. However, a combined wing + jet system can easily have $e_{\rm vector} > 1$ indicating a synergistic benefit of the combination in increasing the overall axial force, or equivalently, in reducing the induced drag. For a planar wing, the limiting upper value of $e_{\rm vector}$ is

$$e_{\rm vector} \;\; \leq \;\; 1 \, + \, \frac{2C_J}{\pi AR} \tag{136}$$

Conversely, if the blowing is unevenly distributed over the span, a much lower $e_{\rm vector}$ is likely to be the result.

6 Sensitivity Analysis

6.1 Operating parameters

The set of operating parameters is defined to be the "global" variables in the Newton system.

$$V_k \quad \Omega_k \quad \mathcal{D}_l \quad \mathcal{P}_l$$

The objective is to determine the sensitivity of all solution quantities with respect to these parameters.

6.2 Circulation sensitivities

The surface flow-tangency residuals (32) and the jet curvature residuals 42) implicitly define the horseshoe vortex strengths Γ_i as functions of the operating parameters.

$$R_i(\Gamma_j, V_k, \Omega_k, \mathcal{D}_l, \mathcal{P}_l) \, = \, 0 \quad \rightarrow \quad \Gamma_j \, = \, \Gamma_j(V_k, \Omega_k, \mathcal{D}_l, \mathcal{P}_l)$$

Taking the variation of R_i we have

$$\delta R_i \;\; = \;\; \frac{\partial R_i}{\partial \Gamma_j} \, \delta\Gamma_j \, + \, \frac{\partial R_i}{\partial V_k} \, \delta V_k \, + \, \frac{\partial R_i}{\partial \Omega_k} \, \delta\Omega_k \, + \, \frac{\partial R_i}{\partial \mathcal{D}_l} \, \delta\mathcal{D}_l \, + \, \frac{\partial R_i}{\partial \mathcal{P}_l} \, \delta\mathcal{P}_l \;\; = \;\; 0 \tag{137}$$

with $R_i = 0$ and hence $\delta R_i = 0$ being required for any physically-correct change. Multiplication by $\left[\frac{\partial R_i}{\partial \Gamma_j}\right]^{-1}$ via LU-decomposition gives the same expressions as the partially-solved Newton system (67), but with $R_i = 0$.

$$\delta\Gamma_i \;\; = \;\; - \, c_{ik}^{V} \, \delta V_k \, - \, c_{ik}^{\Omega} \, \delta\Omega_k \, - \, c_{il}^{\mathcal{D}} \, \delta\mathcal{D}_l \, - \, c_{il}^{\mathcal{P}} \, \delta\mathcal{P}_l \tag{138}$$

The above variational statement implies that the partial derivatives of all the circulations $\Gamma_j(V_k, \Omega_k, \mathcal{D}_l, \mathcal{P}_l)$ are as follows.

$$\frac{\partial \Gamma_i}{\partial V_k} \;\; = \;\; -c_{ik}^{V} \tag{139}$$

$$\frac{\partial \Gamma_i}{\partial \Omega_k} \;\; = \;\; -c_{ik}^{\Omega} \tag{140}$$

$$\frac{\partial \Gamma_i}{\partial \mathcal{D}_l} \;\; = \;\; -c_{il}^{\mathcal{D}} \tag{141}$$

$$\frac{\partial \Gamma_i}{\partial \mathcal{P}_l} \;\; = \;\; -c_{il}^{\mathcal{P}} \tag{142}$$

6.3 Force and moment sensitivities

The sensitivities of forces to operating parameters is obtained by direct linearization of the force expressions. For example, the sensitivity of the inviscid force on a vortex element (79), to a freestream component V_k, is computed as follows.

$$\mathbf{F}_{\mathrm{inv}_i} = \rho\Gamma_i \, \mathbf{W}'_i \times \boldsymbol{\ell}_i \tag{143}$$

$$\frac{\partial \mathbf{F}_{\mathrm{inv}_i}}{\partial V_k} = \rho \frac{\partial \Gamma_i}{\partial V_k} \, \mathbf{W}'_i \times \boldsymbol{\ell}_i \; + \; \rho\Gamma_i \frac{\partial \mathbf{W}'_i}{\partial V_k} \times \boldsymbol{\ell}_i \tag{144}$$

where the two partial derivatives on the righthand side are known from available quantities defined earlier.

$$\frac{\partial \Gamma_i}{\partial V_k} = -c^V_{ik} \tag{145}$$

$$\frac{\partial \mathbf{W}'_i}{\partial V_k} = \sum_j \hat{\mathbf{v}}'_{ij} \left(-c^V_{jk} \right) \; + \; \hat{\mathbf{w}}'^V_{ik} \; + \; \hat{\mathbf{e}}_k \tag{146}$$

The last equation above is obtained directly from (76). All other sensitivities, e.g. with respect to Ω_k, are obtained in an analogous manner. The sensitivities of the total force and moment are the sum of all the element sensitivities.

$$\frac{\partial \mathbf{F}_{\mathrm{inv}}}{\partial V_k} = \sum_i \frac{\partial \mathbf{F}_{\mathrm{inv}_i}}{\partial V_k} \tag{147}$$

The total force and moment sensitivites are used for calculation of standard stability and control derivatives, after suitable axis rotation and normalization.

References

[1] J. Katz and A. Plotkin. *Low-Speed Aerodynamics, 2nd Edition.* Cambridge University Press, Cambridge, U.K., 2001.

[2] C.E. Lan. A quasi-vortex-lattice method in thin wing theory. *Journal or Aircraft*, 11(9), 1974.

[3] E.C. Maskell and D.A. Spence. A theory of the jet flap in three dimensions. *Proceedings of the Royal Society*, 251, 1959.

[4] B. Thwaites. *Incompressible Aerodynamics.* Oxford University Press, Oxford, U.K., 1960. ISBN 0-486-65465-6.